3D REGISTRATION AND MODELLING FOR FACE RECOGNITION

Li Bai, Yi Song
School of Computer Science and Information Technology
University of Nottingham, Jubilee Campus, Wollaton Road,
Nottingham NG8 1BB, UK

Keywords: Registration, modelling, surface reconstruction, recognition.

Abstract This paper presents a new approach to automatic 3D face recognition using a model-based approach. This work uses real 3D dense point cloud data acquired with a stereo face scanner. Since the point clouds are in varied orientations, by applying a non-iterative registration technique, we automatically transform each point cloud to a canonical position and detect facial features used for defining the frontal part of face which is to be modelled in next step. Unlike the iterative ICP algorithm, our non-iterative registration process is scale invariant. An efficient B-spline surface-fitting technique is developed to represent 3D faces in a way that allows efficient surface comparison. This is based on a novel knot vector standardisation algorithm to allow one-to-one mapping from the object space to a parameter space. Consequently, correspondence between objects is established based on shape descriptors, which can be used for recognition.

1 INTRODUCTION

Recent theoretical and technical advance in 3D data capture opens up the possibility of overcoming the difficulties in 2D face recognition systems due to pose and illumination variations. Whereas most of previous works use 2.5D (range) face images, this work uses real three-dimensional (3D) data acquired using a stereo vision based scanner. However, 3D data (dense point clouds in this case) cannot be used directly for shape analysis. First, the objects are in varied orientations and sizes. Second, the surface captured varies significantly across subjects and often includes neck or shoulders. Third, since a data set has around 30,000 vertices, it is impractical using these vertices directly for recognition purposes. Thus we are looking for a compact way to represent face models so that they can be compared.

In this paper, a new approach to efficient 3D face representation from unstructured point clouds is presented. The paper is organised as follows. Section 2 describes our algorithms for simultaneous scale invariant pose estimation and facial features detection. Section 3 presents an efficient B-spline surface reconstruction method, from which shape descriptors are obtained to represent all face models in a parameter space. With the affine-invariant property of shape descriptors, normalisation and alignment can be easily done as discussed in section 4. Correspondences between objects are also obtained via the one-to-one mapping from the object space to a parameter space. The distance metric is then developed for face recognition. Finally, section 5 concludes the paper with the future research directions.

2 REGISTRATION

2.1 Previous Work

In the past, several efforts have been made for the registration of 3D point clouds. One of the most popular methods is the iterative closest point (ICP) algorithm developed by Besl and McKay (1992). The ICP searches a pair of nearest points in two data sets, and estimates a rigid transformation which aligns the two points. The rigid transformation is then applied to all the points of one data set to try to match those of the second, and the procedure is iterated until some optimisation criteria is satisfied. Several variations of the ICP method have been proposed. Chen and Medioni (1992) evaluated the

Bai L. and Song Y. (2006).
3D REGISTRATION AND MODELLING FOR FACE RECOGNITION.
In *Proceedings of the First International Conference on Computer Vision Theory and Applications*, pages 201-208
DOI: 10.5220/0001371002010208

registration function using point-to-plane distance. In Zhang (1994), a robust statistic threshold was introduced to determine the matching distance dynamically. Iterative methods such as this are obviously time consuming. When the assumption of one data set being a subset of the other is not valid, false matches can be created (Fusiello et al, 2002). Moreover, they rely on a good estimate of the initial transformation. Another deficiency of the ICP method is scale sensitive. There are other alternative approaches. For example, some feature-based registration methods were presented in (Godin et al, 1994; Godin and Boulanger, 1995; Godin et al, 2001). More detailed reviews on registration can be found in (Campbell and Flynn, 2001; Flusser and Zitova, 2003).

In face recognition, we have to register face scans of varied sizes due to either the distinct characteristics of each individual, e.g. faces between child and adult, or the scale change of a scanner. Moreover, the face surface varies significantly across subjects and often includes neck or shoulders. Finally, no transformation can be reasonably estimated to pre-align two face scans.

2.2 Our Approach

The aim of registration is to define a transformation, which takes a face of an arbitrary view to a canonical position. The transformation can be written as:

$$D' = k \cdot R \cdot D + t \qquad (1)$$

where D and D' are the observed data before and after transformation, respectively. R is a 3×3 rotation matrix. The translation t and normalisation k can be done using shape descriptors obtained from surface reconstruction in section 3. The task at this stage is to automatically find the rotation matrix, such that D* = RD is in the canonical position. The rotation matrix represents the pose estimate of the original data set. The canonical position is defined as (in world coordinate system), see Figure 2(c):

- The line linking two inner eye corners (E_{left}, E_{right}) is perpendicular to the yz plane after registration;
- The facial symmetry plane I is perpendicular to the xy plane passing through nose tip $N_{tip.}$
- Both nose top N_{top} and nose bottom N_{bottom} are located in plane I, and the line linking them is perpendicular to the xz plane.

N_{top} is defined as the intersection of the line linking E_{left} and E_{right} and plane I . The nose tip can be located during clouds generation.

Two stages are involved to obtain the rotation matrix R and facial features. The first stage is to estimate the initial rotation matrix (head pose) based on the symmetry property of a face. Briefly, B-spline curves are fitted to the point cloud, and the resulting B-spline curves are measured against the canonical coordinate axes to determine their deviations from each axis to estimate the rotation about that axis. The rotation matrix is the composite of rotations around all the axes:

$$R_{app} = R_{zi} \cdot R_{yi} \cdot R_{xi} \qquad (2)$$

Data will be near frontal after being transformed by R_{app}. Figure 1(a) illustrates the initial pose estimation procedure and the result.

The next stage is to detect facial features and refine the initial pose estimate, as shown in Figure 1(b). The nose saddle point is estimated first. Possible areas containing inner corners of the eyes can then be decided upon, as shown in Figure 1(c). For each area, eight candidates of the inner eye corners are obtained for further consideration. The pair of points with the highest priority value is chosen as the inner eye corners. Feature detection and pose refinement are done in parallel, since the coordinates of these features are directly related to pose.

Pose refinement uses the following rotation matrix:

$$R_{re} = R_x \cdot R_y \cdot R_z \qquad (3)$$

where R_x, R_y and R_z are the compensation rotation matrices around x, y and z axes. The key idea of pose refinement is to evaluate R_x, R_y and R_z using the facial feature points. As D* will be in the canonical position after transforming the original data with R= $R_{re} \bullet R_{app}$, feature points must satisfy the equations (4)-(10) simultaneously:

$$\exists N_{top,x} \cdot \left\{ \begin{array}{l} N_{top,x} = \dfrac{(R_y R_z E_{left,x}{}' + R_y R_z E_{right,x}{}')}{2} \\ \mathrm{I} \ \min\limits_{n^2} \left\{ \left\| N_{top,x} - N_{tip,x} \right\| \right\} \end{array} \right\} \qquad (4)$$

where $E_{left}{}'$ and $E_{right}{}'$ are the candidate pair of inner eye corners; n is number of candidate inner eye corners

$$N_{top,y} = R_y R_z E_{left,y} = R_y R_z E_{right,y} = \sum_{i=0}^{m} B_{i,p}(s') C_{i,y} \qquad (5)$$

$$N_{top,z} = \sum_{i=0}^{m} B_{i,p}(s') C_{i,z} \qquad (6)$$

$$N_{bottom,x} = N_{tip,x} \qquad (7)$$

$$N_{bottom,y} = \sum_{i=0}^{m} B_{i,p}(s'')C_{i,y} \qquad (8)$$

$$N_{bottom,z} = \sum_{i=0}^{m} B_{i,p}(s'')C_{i,z} \qquad (9)$$

$$R_z N_{top,z} = R_z N_{bottom,z} \qquad (10)$$

where $\sum_{i=0}^{m} B_{i,p}(s)C_i$ represents the face profile inferred from the facial symmetry plane.

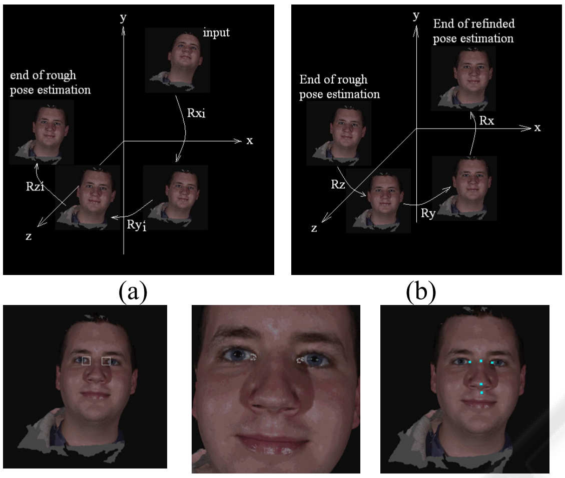
y
input
end of rough pose estimation
Rxi
x
Rzi
Ryi
z
y
End of refinded pose estimation
End of rough pose estimation
Rx
x
Rz
Ry
z

(a) (b)

© (d) (e)

Figure 1: Procedures of pose estimation and facial features detection. (a) Initial pose estimate. (b) Refined pose estimate. (c) Output from the first stage of pose estimation. Possible areas containing the inner corner of eyes are decided upon. (d) Candidates of the inner eye corners chosen from the areas marked in (c). (e) Detected facial features and the final output from the pose estimation algorithm.

Figure 2 shows an example result of registering original point clouds to a canonical position.

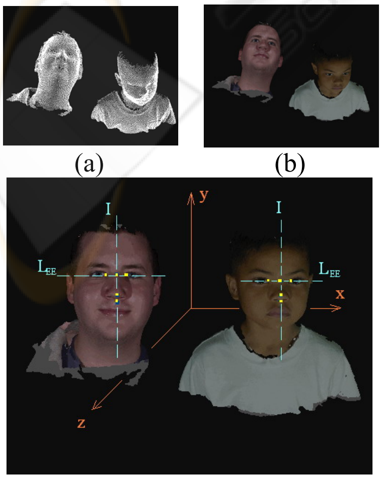

(a) (b)

(c)

Figure 2 Examples of original point clouds before and after applying our registration algorithm. (a) Input point clouds acquired from 3D scanner with varied orientations. (b) Input point clouds displayed in texture. (c) Output point clouds in the canonical position (in a same orientation).

We will now compare our 3D registration methods with the ICP algorithm. The ICP registration results are shown in Figure 3 (b) and (e). Figure 3 (c) and (f) are the results using our approach.

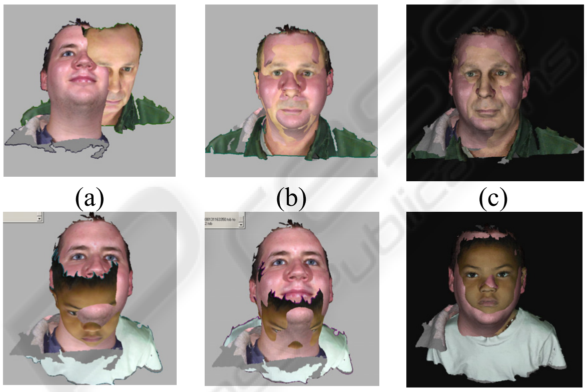

(a) (b) (c)

(d) (e) (f)

Figure 3: Comparison between ICP method and our proposed method. (a) First pair of point clouds to be registered. (b) Positive result from ICP method. (c) The registration result using our approach. (d) Second pair of input point clouds. (e) Negative result from ICP algorithm. (f) Our result.

3 3D MODELLING

The 3D modelling problem can be stated as follows: given a unstructured point cloud P: pi (xi, yi, zi), find a B-spline surface F: R2 → R3, which fits the point cloud best.

There has been considerable work on fitting B-spline surfaces to 3D points. However, most work dealt with fitting a single B-spline patch on a regular grid data set. This can only deal with simple data sets, e.g. a deformed quadrilateral (Hoschek et al, 1989; Rogers and Fog, 1989; Sarkar and Menq, 1991) or a deformed cylinder (Schmitt et al, 1986). To reconstruct complex surfaces, many efforts focus on interconnecting multiple surface patches (Eck et al, 1995; Eck and Hoppe, 1996; Krishnamurthy and Levoy, 1996; Milroy et al, 1995). The problem with this is the difficulty in having all objects modelled in the same parameter space, since every patch has its own parameter space.

Our aim is to construct a compact and unique representation of the 3D surface to allow face comparison. This is achieved by constructing, automatically, a single B-spline surface having C^{k-1} continuity (k is the degree of B-spline function) everywhere intrinsically, Figure 4(b), rather than many patches stitched together. This makes object comparison impossible.

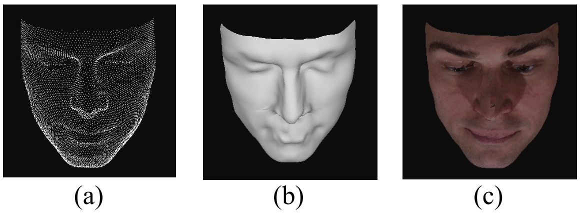

Figure 4: 3D modelling. (a) Unstructured point cloud to be reconstructed. (b) Reconstructed surface. (c) Reconstructed surface with texture mapping.

The procedure of constructing this single B-spline surface is as follows:

- Decomposing the surface-fitting problem to a sequence of curve-fitting problems based on a knot vector standardisation algorithm. We reconstruct a single B-spline surface on a parameter space by the control points of the surface and individual knot vectors. This is discussed in section 3.2.
- Since the B-spline surface obtained from section 3.2 depends on the control points, parameter values and basis functions, which vary from individual to individual, there is no direct mapping from the parameter domain to the object space. The task in section 3.3 is to obtain a direct one-to-one mapping relationship from the object space to the parameter domain.

3.1 Knot Vector Standardisation

Given n_X+1 control points ***f**: {f_1, f_2, …, f_{nX}}* and a knot vector $X=\{x_0, x_1, \ldots, x_{nx+g+1}\}$, the B-spline curve F of degree g is:

$$F(x) = \sum_{i=0}^{n_X} B_{i,g}(x) f_i \qquad (11)$$

$$B_{i,g}(x) = \frac{x - x_i}{x_{i+g} - x_i} B_{i,g-1}(x) + \frac{x_{i+g+1} - x}{x_{i+g+1} - x_{i+1}} B_{i+1,g-1}(x)$$

Another B-spline curve L defined by n_Y+1 control points ***l**: {l_1, l_2, …, l_{ny}}* and a distinct knot vectors $Y=\{y_0, y_1, \ldots, y_{ny+g+1}\}$ is:

$$L(y) = \sum_{j=0}^{n_Y} N_{j,g}(y) l_j \qquad (12)$$

$$N_{j,g}(y) = \frac{y - y_j}{y_{j+g} - y_j} N_{j,g-1}(y) + \frac{y_{j+g+1} - y}{y_{j+g+1} - y_{j+1}} N_{j+1,g-1}(y)$$

The task is to standardise distinct knot vectorsand have B-spline curves F and L defined on the same knot vector.

Instead of simply merging all knot vectors together (Watt and Watt, 1992), our approach is to standardise all knot vectors to a pre-defined knot vector $U=\{u_0, u_1, \ldots, u_{nu+g+1}\}$. Correspondingly, control points set $\{f_i\}$ is re-calculated as

$$\overset{n_X}{\underset{i=0}{f}} \ \alpha \ \overset{n_U}{\underset{k=0}{f'}} \qquad (13)$$

Then curve F is:

$$F'(x) = \sum_{k=0}^{n_U} B'_{k,g}(x) f'_k \qquad (14)$$

$$B'_{k,g}(x) = \frac{x - u_k}{u_{k+g} - u_k} B'_{k,g-1}(x) + \frac{u_{k+g+1} - x}{u_{k+g+1} - u_{k+1}} B'_{k+1,g-1}(x) \qquad (15)$$

Similarly, we have curve L defined on the same knot vector U by

$$\overset{n_Y}{\underset{j=0}{l}} \ \alpha \ \overset{n_U}{\underset{k=0}{l'}} \qquad (16)$$

$$L'(y) = \sum_{k=0}^{n_U} N'_{k,g}(y) l'_k \qquad (17)$$

$$N'_{k,g}(y) = \frac{y - u_k}{u_{k+g} - u_k} N'_{k,g-1}(y) + \frac{u_{k+g+1} - y}{u_{k+g+1} - u_{k+1}} N'_{k+1,g-1}(y) \qquad (18)$$

Comparing Equation (17) and (20), it is obvious that the basis functions B' and N' are identical. We then have one basis function expression Q for all B-spline curves defined upon the knot vector U:

$$Q_{k,g}(s) = \frac{s - u_k}{u_{k+g} - u_k} Q_{k,g-1}(s) + \frac{u_{k+g+1} - s}{u_{k+g+1} - u_{k+1}} Q_{k+1,g-1}(s) \qquad (19)$$

Consequently, Equation (11) and (12) can be rewritten as:

$$F'(s) = \sum_{k=0}^{n_U} Q_{k,g}(s) f'_k \qquad (20)$$

$$L'(s) = \sum_{k=0}^{n_U} Q_{k,g}(s) l'_k \qquad (21)$$

Errors ***E*** is measured between the set of original data points D and the corresponding interpolated values from B-spline curve F'. s_d is the parameter value associated with data point d. Then, we can define ***E*** to be

$$E = \underset{d \in D}{\mathrm{Y}} \frac{\left\| d - F'(s_d) \right\|}{d} \qquad (22)$$

The maximum error was within 1%. Therefore we could ignore the difference between curve F' and F, by having F' ≈ F.

3.2 B-spline Surface Fitting

A B-Spline surface

$$\Gamma(s,t)=\sum_{j=0}^{n}\sum_{i=0}^{m}B_{j,g}(s)N_{i,h}(t)C_{i,j} \qquad (23)$$

is defined by

- a set of m+1 rows and n+1 column control points $C_{i,j}$, where $0 \le i \le m$, and $0 \le j \le n$;
- a knot vector of l+1 knots in the u- direction, $U=\{u_0, u_1, \ldots, u_l\}$;
- a knot vector of k+1 knots in the v- direction, $V=\{v_0, v_1, \ldots, v_k\}$;
- degree h in the u- direction; and
- degree g in the v- direction.

$B_{j,g}(s)$ is the B-Spline basis functions in the u-directions, defined over knot vector U:

$$B_{j,0}(s)=\begin{cases}1 & \text{if } u_j \le s < u_{j+1}\\ 0 & \text{otherwise}\end{cases} \qquad (24)$$

$$B_{j,g}(s)=\frac{s-u_j}{u_{j+g}-u_j}B_{j,g-1}(s)+\frac{u_{j+g+1}-s}{u_{j+g+1}-u_{j+1}}B_{j+1,g-1}(s) \qquad (25)$$

$N_{i,h}(t)$ is defined analogously over the knot vector V in the v-direction.

Given grid data **P**: $\{p_{c,d} \mid p_{c,d} \in R^3, 0 < c < m, 0 < d < n\}$, uniform knot vector U and V are obtained for the u- and v- direction, respectively, basing on the property of grid data spacing at equal intervals. In this case, the fundamental identities, i.e. l=m+h+1 and k=n+g+1, can be held explicitly for the pair knot vector U and V. Then the problem of finding the underlying B-Spline surface Γ fitting **P** best can be converted into a sequence of curve fitting processes (Schmitt et al, 1986). However, for a complex surface, e.g. face in Figure 4 (a), obtaining grid data on all areas such as forehead, nose and chin etc. is a nontrivial problem. Alternative approaches are to divide the surface into small planar patches and then re-sample each patch to get grid data (Krishnamurthy and Levoy, 1996; Milroy et al, 1995; Eck and Hoppe, 1996), which require extensive computation subdividing the surface and maintaining continuity.

By applying the knot vector standardisation algorithm described in 3.1, fundamental identity can also be enforced on non-grid data. Thus non-grid data can be decomposed into small portions upon which the curve-fitting procedure can be applied independently, as does on grid data. Consequently, we can apply different automatic sampling schemes on different parts of a face. For example, the forehead area is rather flat with little curvature changes. A sparse and evenly sampling scheme will work well. In contrast, the area close to the nose contains sharp curvature variations. A dense and uneven sampling scheme is necessary to guarantee precise interpolation.

Following the discussion above, the point cloud data $\overline{P}:\{p \in R^3\}$ are decomposed into small portions $\overline{P}:\{\overline{p}_0, \overline{p}_1, \Lambda\ \overline{p}_m\}$ (sub dataset), where, $\overline{p}_0:\{p_{0,0}, p_{0,1}, \Lambda\ p_{0,x0}\}$, …, $\overline{p}_m:\{p_{m,0}, p_{m,1}, \Lambda\ p_{m,xm}\}$ and $x_0 \ne x_1 \ne \ldots x_m$. For each sub dataset $\overline{p}_c$, $0 \le c \le m$, the curve-fitting procedure is applied independently:

$$p_{cd}=\sum_{d=0}^{xc}B_{d,g}(s_d)Q_{cd} \qquad (26)$$

After standardising knot vectors, Equation 26 is written as

$$p_{cd}=\sum_{j=0}^{n}B_{j,g}(s_d)Q_{c,j} \qquad (27)$$

where $$Q_{c,j}=\sum_{i=0}^{m}N_{i,h}(t_c)C_{i,j} \qquad (28)$$

From Equation 27 and 28, the underlying B-Spline surface is calculated as:

$$\begin{aligned}p_{cd}&=\sum_{j=0}^{n}B_{j,g}(s_d)\Big(\sum_{i=0}^{m}N_{i,h}(t_c)C_{i,j}\Big)\\&=\sum_{j=0}^{n}\sum_{i=0}^{m}B_{j,g}(s_d)N_{i,h}(t_c)C_{i,j}=\Gamma(s_d,t_c)\end{aligned} \qquad (29)$$

3.3 Shape Descriptors

After B-spline surface-fitting, we have each face modelled by a set of control points over its own pair of knot vectors. If we use matrix operations to present the reconstructed B-spline surface, i.e. Equation (23), we have:

$$\Gamma^k(s,t)=A(\overset{k}{B}(s),\overset{k}{N}(t))\bullet vec(\overset{k}{C}) \qquad (30)$$

where matrix A represents the Kronecker product. Obviously Equation (30) is not a direct function of parameter (s, t) yet. By applying knot vector standardisation, we can remove the dependency on individual knot vectors in Equation (30). By having

$$A(\overset{k}{B}(s),\overset{k}{N}(t))\ \alpha\ \overset{-}{A}(s,t) \qquad (31)$$

$$vec(\overset{k}{C})\ \alpha\ \overset{k}{C'} \qquad (32)$$

where $\bar{A}$ is a function of (s,t) for all face models. $\overset{k}{C'}$ is a set of parameters ∈ R^3 which is independent of individual knot vectors, we arrived at

$$\Gamma^k(s,t) = \bar{A}(s,t)\cdot\overset{k}{C'} \qquad (33)$$

Thus we have established a direct mapping between the parameter domain (s, t) ∈ Ω: [0,1]×[0,1] and the object space Γ ∈ R^3. From Equation (33), we know that C' defines the unique shape of a surface, i.e. C' is a shape descriptor. Figure 4(b) shows a rendered B-spline surface using shape descriptors over the domain Ω. Shape descriptors have several important properties, including:

- Establishing direct one-to-one mapping relationship from the parameter domain to the object space. For each pair of parameter value (s, t), we have a unique corresponding B-spline surface point in the object space.
- Compact representation for 3D objects. The approach can achieve over 90% compression rate with similar rendering result to polygon representation.
- Affine-invariance. The same result will be obtained transforming a B-spline surface itself or its shape descriptors. This is a very important property and will be used in next section for normalisation and alignment. Instead of translating and scaling the 3D object directly, we will apply the operations to its shape descriptors.

4 FACE RECOGNITION

We have represented 3D face scans in a form which can be used to compare faces. In this section, we will use this representation to match test faces to those stored in a database. Currently, our database consists of 30 individuals, 3 scans per individual. One scan is used to construct the 3D face database, whilst the other 2 scans are used in face recognition experiments. The test set consisted of 24 individuals with 2 scans for each.

Each face in the database and test set is modelled using the techniques discussed in previous sections. Each object in the test set is compared against all the faces in the database. The face having the smallest difference is identified as the best match to the test face. The procedure is shown in Figure 5. Details of the implementation is described below.

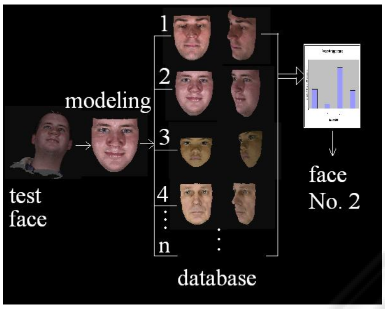

Figure 5: Face recognition based on the distance metric.

4.1 Face Comparison

We normalise and align face models first. As mentioned in section 3, normalisation and alignment can be done fairly straightforwardly using the affine-invariant property of shape descriptions. Taking one model in the database as the generic model, we normalise and align all the face models to the generic model.

$$\overset{k}{C''} = k\cdot\overset{k}{C'} + t \qquad (34)$$

where k and t are scalars of normalisation and translation, respectively. The normalised and aligned face model is:

$$\Gamma^k(s,t) = \bar{A}(s,t)\cdot\overset{k}{C''} \qquad (35)$$

The corresponding surface points between models can be generated due to the one-to-one mapping from the parameter domain Ω to the object space. For each pair of parameters (s, t), each face model has a unique corresponding B-spline surface point:

$$(s,t) \Rightarrow \Gamma^k(s,t) \qquad (36)$$

$$(s,t) \Rightarrow \Gamma^{k+1}(s,t) \qquad (37)$$

Therefore, B-spline surface points Γ^k(s, t) and Γ^{k+1}(s, t) are uniquely mapped, i.e.

$$\Gamma^k(s,t) \Rightarrow \Gamma^{k+1}(s,t) \qquad (38)$$

Examples are shown in Figure 6.

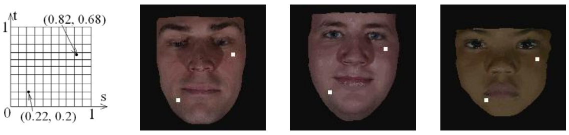

(a) (b) (c) (d)

Figure 6:Corresponding B-spline surface points. (a) A common parameter domain Ω. (b)-(d) Face models reconstructed on the parameter domain, Ω in (a). For each

parameter pair marked in (a), there is a unique surface point on each face model.

By sampling the parameter domain, we obtain a set of corresponding B-spline surface points on each face model. The linear distance-based method, i.e. Euclidean distance matrix analysis (EDMA) (Lele ans Richtsmeier, 2001) can be used as metric to judge the similarity between a test face and each face in a database, which is given by

$$\min_{i=0}^{N}\left\{\sum_{t=0}^{n}\sum_{s=0}^{m}\left(\begin{array}{l}\left\|\Gamma^{i}(s,t)-\sum_{\substack{t'\neq t\\ t'=0}}^{n}\sum_{\substack{s'\neq s\\ s'=0}}^{m}\Gamma^{i}(s',t')\right\| \\ -\left\|\Gamma^{test}(s,t)-\sum_{\substack{t'\neq t\\ t'=0}}^{n}\sum_{\substack{s'\neq s\\ s'=0}}^{m}\Gamma^{test}(s',t')\right\|\end{array}\right)\right\} \qquad (39)$$

where Γ^{i} represents the ith model in the database; Γ^{test} is a test object which we want to find its matching face model in the database. N is the total numbers of the 3D models in the database. Small values indicate a high degree of similarity.

4.2 Experimental Results

The representative 3D models and test scans are shown in Figure 7 and Figure 8 respectively.

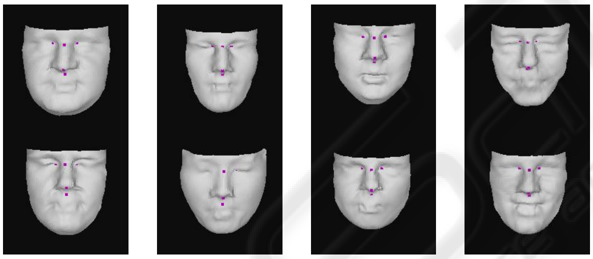

Figure 7: Some of the 3D face models in the database.

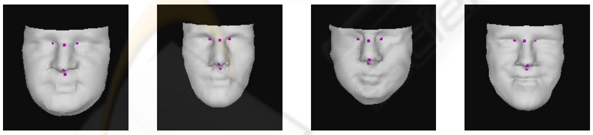

Figure 8: Representative test faces.

Each face in the data set is compared against all the 3D models in the database. The examples of similarity measurement between test faces and each face in a database are provided in Figure 9.

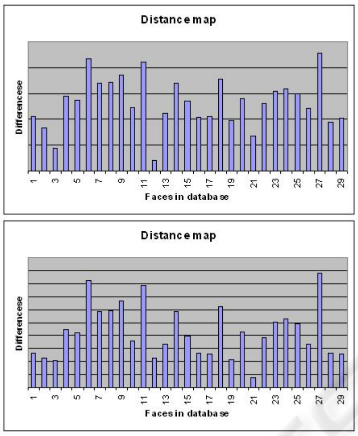

Figure 9: Similarity measurement. The bar charts show the similarity between a test face and each face in a database. The face having the smallest difference to the test face is identified as the best match to the test face.

Out of the 4 errors in the 48 test faces (corresponding to 91.7% accuracy), 2 test faces are different scans of the same subject with different facial expressions. In the other two cases, the correct match is ranked the second best, Figure 10(top). However, incorporating some additional information, e.g. using the square root distance between corresponding points as an additional metric to compare the similarity, given by Equation 40, they are correctly identified, Figure 10(bottom).

$$\min_{i=0}^{N}\left\{\sum_{t=0}^{n}\sum_{s=0}^{m}\left\|\Gamma^{i}(s,t)-\Gamma^{test}(s,t)\right\|^{2}\right\} \qquad (40)$$

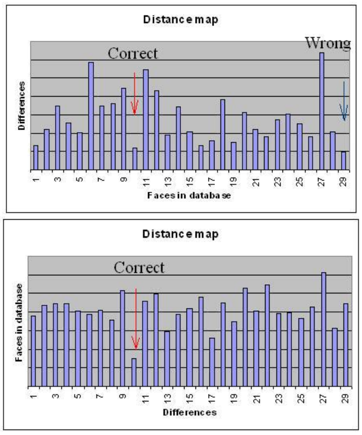

Figure 10: The difference between the test face and the impostor face. (Top) The correct model is the second ranked face in the database. (Bottom) Result after combining another recognition strategy.

5 CONCLUSION

We have developed a new automatic model-based face recognition system, which includes both non-iterative registration and the representation of 3D face models by shape descriptors. By registering point clouds to a canonical position, we overcome the pose-variation problem. Unlike ICP algorithm, this non-iterative registration process is scale invariant. An efficient B-spline surface-fitting technique is developed to reconstruct underlying surface for the registered data set. A new knot vector standardisation technique is proposed to allow a direct one-to-one mapping relationship from the object space to a parameter space. Subsequently, a compact parametric representation of 3D objects is obtained. The system has been tested on a personal computer (Pentium 4/512M RAM). Compared with the existing method of closed surface parameterisation, which takes 33s to 536s depending on the complexity of the objects [BGK96], the registration and modelling process introduced in this paper only takes 2 seconds, on an average sized point cloud (about 25,000 vertices).

Although surface distance can be used as a metric for face recognition, it may not be very sufficient since no explicit geometric information is employed. Our future work is to integrate geometric information into recognition methods. For example, we may turn a recognition problem into a classification problem of the shape descriptors.

With the proposed surface representation, it is possible to analyse facial component separately. As the geometry of B-spline surface can be inferred from the shape descriptors, we can delineate facial areas, e.g. forehead, nose, mouth, chin, from the parameter space, and weigh each part separately in the recognition metric to reduce the influence of facial expression. The areas potentially affected by facial expression will be given lower weight.

REFERENCES

Besl, P.J., and McKay, N.D. (1992) A Method for Registration of 3D Shapes. IEEE Pattern Analysis and Machine Intelligence, vol. 14, No. 2, 239-256.

Chen, Y., and Medioni, G. (1992) Object modelling by registration of multiple range images. Image and Vision Computing, vol. 10, No. 3, 145-155.

Campbell, R., Flynn, P. (2001) A Survey of Free-form Object Representation and Recognition Techniques, Computer Vision and Image Understanding, vol. 81, pp. 166-210.

Eck, M., DeRose, T., Duchamp, T., Hoppe, H., Lounsbery, M., and Stuetzle, W. (1995) Multiresolution Analysis of Arbitrary Meshes. In Computer Graphics (Proceedings of SIGGRAPH’ 95), pages 173-182.

Eck, M., and Hoppe, H. (1996) Automatic Reconstruction of B-Spine Surfaces of Arbitrary Topological Type. Proc. 23rd Int'l. Conf. on Computer Graphics and Interactive Techniques SIGGRAPH '96, ACM, New York, NY. pp. 325-334.

Fusiello, A., Castellani, U., Ronchetti, L., and Murino, V. (2002) Model Acquisition by Registration of Multiple Acoustic Range Views, Computer Vision, ECCV2002, Springer, pp. 805-819.

Flusser, J. and Zitova, B. (2003) Image Registration Methods: A Survey, Image and Vision Computing, vol. 21, pp. 977-1000.

Godin, G. and Boulanger, P. (1995) Range Image Registration Through Viewpoint Invariant Computation of Curvature, IAPRS, 30 (5/W1), pp. 170-175.

Godin, G., Rioux, M. and Baribeau, R. (1994) Three-dimensional Registration Using Range and Intensity Information, SPIE, vol. 2350, Videometrics III, pp. 279-290.

Godin, G., Laurendeau, D. and Bergevin, R. (2001) A Method for the Registration of Attributed Range images, International Conference on 3D Imaging and Modeling, Quebec, pp. 179-186.

Hoschek, J., Schneider, F. –J. and Wassum, P. (1989) Optimal Approximate Conversion of Spline Surfaces, Computer Aided Geometric Design, vol. 6, issue 4, pp. 293-306.

Krishnamurthy, V. and Levoy, M. (1996) Fitting Smooth Surfaces to Dense Polygon Meshes, ACM-0-89791-746-4/96/008.

Lele, S. and Richtsmeier, J. (2001) An Invariant Approach to the Statistical Analysis of Shapes. Boca Raton: Chapman & Hall/CRC.

Milroy, M., Bradley, C., Vickers, G. and Weir, D. (1995) G1 Continuity of B-spline Surface Patches in Reverse Engineering. CAD 27, 471-478.

Rogers, D. and Fog, N. (1989) Constrained B-spline Curve and Surface Fitting, Computer Aided Design, vol. 21, pp. 641-648.

Schmitt, F., Barsky, B. and Du, W. H. (1986) An Adaptive Subdivision Method for Surface Fitting from Sampled Data. Computer Graphics (SIGGRAPH’ 86 Proceedings), volume 20. pp. 179-188.

Sarkar, B. and Menq, C. (1991) Parameter Optimization in Approximating Curves and Surfaces to Measurement Data, Computer Aided Geometric Design, vol. 8, pp. 267-290.

Watt, A. and Watt, M. (1992) Advanced Animation and Rendering Techniques: Theory and Practise. Addison-Wesley.

Zhang, Z. (1994) Iterative Point Matching for Registration of Free-form Curves and Surfaces. International Journal of Computer Vision, vol. 13, No. 2, pp.119-152.